

Current fluctuations in non-interacting run-and-tumble particles in one-dimension

Tirthankar Banerjee,^{1,2} Satya N. Majumdar,¹ Alberto Rosso,¹ and Grégory Schehr¹

¹*LPTMS, CNRS, Univ. Paris-Sud, Université Paris-Saclay, 91405 Orsay, France*

²*Instituut voor Theoretische Fysica, KU Leuven, 3001 Heverlee, Belgium*

(Dated: February 8, 2021)

We present a general framework to study the distribution of the flux through the origin up to time t , in a non-interacting one-dimensional system of particles with a step initial condition with a fixed density ρ of particles to the left of the origin. We focus principally on two cases: (i) when the particles undergo diffusive dynamics (passive case) and (ii) run-and-tumble dynamics for each particle (active case). In analogy with disordered systems, we consider the flux distribution both for the annealed and the quenched initial conditions, for the passive and active particles. In the annealed case, we show that, for arbitrary particle dynamics, the flux distribution is a Poissonian with a mean $\mu(t)$ that we compute exactly in terms of the Green's function of the single particle dynamics. For the quenched case, we show that, for the run-and-tumble dynamics, the quenched flux distribution takes an anomalous large deviation form at large times $P_{\text{qu}}(Q, t) \sim \exp\left[-\rho v_0 \gamma t^2 \psi_{\text{RTP}}\left(\frac{Q}{\rho v_0 t}\right)\right]$, where γ is the rate of tumbling and v_0 is the ballistic speed between two successive tumblings. In this paper, we compute the rate function $\psi_{\text{RTP}}(q)$ and show that it is nontrivial. Our method also gives access to the probability of the rare event that, at time t , there is no particle to the right of the origin. For diffusive and run-and-tumble dynamics, we find that this probability decays with time as a stretched exponential, $\sim \exp(-c\sqrt{t})$ where the constant c can be computed exactly. We verify our results for these large deviations by using an importance sampling Monte-Carlo method.

I. INTRODUCTION

Current fluctuations in non-equilibrium open systems has been a major area of research in statistical physics over the last few years [1–9]. The probability distribution of the current of particles across a given point in space typically admits a large deviation form and the corresponding large deviation function (rate function) is often interpreted as an analogue of a free energy in non-equilibrium systems. For example, it was shown in [1] that for a large one dimensional system in contact with reservoirs at unequal densities at the two ends, there exists an additivity principle obeyed by the large deviation function, much like the free energy in equilibrium systems. This additivity principle has been exploited further to compute cumulants of the current distribution [1–8]. Several theoretical tools have been developed to study current fluctuations, notable among them is the Macroscopic Fluctuation Theory [1, 3, 6, 9] and the Bethe Ansatz [7]. Most of these studies have focused on driven diffusive systems, both interacting (as in the simple symmetric exclusion process) and non-interacting, typically in a one-dimensional setting.

Another inherently out-of-equilibrium system, much studied recently, is the so-called *active* run-and-tumble particle (RTP) [10–13], a new incarnation of the persistent random walk [14, 15]. Such motion has been observed in certain bacteria such as *E. Coli* where the bacterium moves in straight runs, undergoes tumbling at the end of a run and chooses randomly a new direction for the next run [10–15]. These motions are inherently out-of-equilibrium since they consume energy directly from the environment and self-propel themselves without any external force. There has been an enormous amount of work concerning the collective properties of an assembly of such RTPs [16–20]. Even at the single-particle level, RTP displays interesting behaviour and several single-particle observables have been studied recently. These include the position distribution for a free RTP [12, 14, 21], non-Boltzmann stationary states for an RTP in a confining potential [19, 22–25], effects of disordered potentials [26], first-passage properties [27–32], the distribution of the time at which an RTP reaches its maximum displacement [33] and RTP subjected to stochastic resetting [34, 35].

However, as far as we are aware, current fluctuations, even in a system of noninteracting RTPs have not been systematically studied. The purpose of this paper is to study the current fluctuations in the simplest setup where RTPs are noninteracting and initially confined on one-half of the real line (i.e. step-function initial condition). Such a setup was used before by Derrida and Gerschenfeld for noninteracting diffusive particles [6] and they were able to compute the large-deviation form of the current or flux Q_t of particles through the origin *up to* time t . In this paper, we use exactly the same setup, but for a more general class of noninteracting particles, which includes both diffusive as well as run-and-tumble particles, and compute analytically the flux distribution up to time t .

Thus the main observable of our interest is the flux Q_t defined as the number of particles that crossed the origin (either from left or right) *up to* time t , starting from the step initial condition where the particles are uniformly distributed over only the left side of the origin. Let us denote its probability distribution by $P(Q, t) = \text{Prob.}(Q_t = Q)$. Clearly Q_t is a history dependent quantity, since it involves counting of all the crossings of the origin up to time t . Our

exact results rely on a simple but crucial observation, valid for this special step initial condition: each particle, starting from the left side of the origin, that crosses the origin an even number of times up to time t does not contribute to the flux Q_t . But if it crosses the origin an odd number of times, it contributes unity to the flux Q_t . Hence, the flux Q_t is exactly equal to the number N_t^+ of particles present on the right side of the origin at time t , i.e. $Q_t = N_t^+$. Thus the history dependent observable Q_t gets related, via this observation, to N_t^+ which is an instantaneous observable at time t . As we will see later, it is much easier to compute the probability distribution $P(N^+, t) = \text{Prob.}(N_t^+ = N^+)$, rather than the distribution of Q_t directly. Hence, knowing the distribution of N_t^+ , we can compute the flux distribution from $P(Q, t) = \text{Prob.}(N_t^+ = Q)$. Note that this equivalence holds for arbitrary dynamics of the particles, for example it holds both for diffusive as well as RTP dynamics of the particles.

Based on this connection $Q_t = N_t^+$, we can apply our results for the flux distribution to another interesting problem. Consider for instance an ideal gas of noninteracting particles in a box. Imagine that the box is divided into two halves by a removable wall. Initially, all the particles are on the left half of the box and at $t = 0$ we lift the wall and let the particles explore the full box freely. At time t , we take a snapshot of the system and observe the locations of the particles. Of course, on an average, one expects that, at long times, the particles will be uniformly distributed throughout the box. We can ask: what is the probability that, at time t , all the particles are again back to the left half of the box? Clearly this is an extremely rare event but what is the probability of this event? How does it decay with time? But note that this is exactly the probability $\text{Prob.}(N_t^+ = 0) = P(Q_t = 0, t)$. Hence, our computation of the flux distribution with step initial condition gives access to the probability of this rare event (corresponding to all the particles coming back to the left half of the box at time t), in a one-dimensional setting.

The rest of the paper is organised as follows. In section II we discuss the model and present a summary of our main results. Then in Sec. III we introduce the general setting and show how the single-particle Green's function plays the central role in the analysis. Next in Secs. IV and V, we calculate the annealed and quenched averages, respectively, of the probability distribution of the flux for both diffusive and run-and-tumble particles. Then in Sec. VI we give the numerical verifications of our results and finally in Sec. VII we summarize and conclude.

II. THE MODEL AND THE MAIN RESULTS

We consider a set of N noninteracting particles initially distributed uniformly with a density ρ on the negative real axis, as in Fig. 1. Without loss of generality, we label the particles $i = 1, 2, \dots, N$ with $x_i(t)$ denoting the position of the i -th particle at time t . Each $x_i(t)$ evolves independently by a stochastic (or deterministic) evolution rule (the same law of evolution for each particle). For example, each particle can undergo independent Brownian motion. Alternatively, each particle can undergo independent RTP dynamics in one-dimension. This RTP dynamics for a single particle is defined as follows.

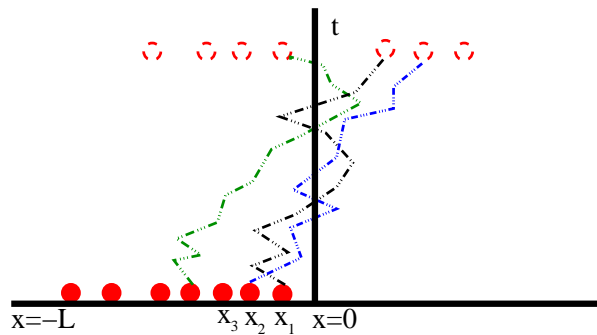


FIG. 1: Schematic representation of an initial realization with all particles on the left of an arbitrary origin ($x = 0$) on an infinite line $L \rightarrow \infty$. After time t each particle undergoes some displacement depending on the dynamics. The quantity of interest in our case is the number of particles on the right of the origin at time t .

RTP dynamics. The position of a single RTP $x(t)$ evolves via the Langevin equation

$$\frac{dx}{dt} = v_0 \sigma(t) \quad (1)$$

where v_0 is the intrinsic speed during a run and $\sigma(t) = \pm 1$ is a dichotomous telegraphic noise that flips from one state to another with a constant rate γ . The effective noise $\xi(t) = v_0 \sigma(t)$ is coloured which is simply seen by computing

its autocorrelation function

$$\langle \xi(t)\xi(t') \rangle = v_0^2 e^{-2\gamma|t-t'|}. \quad (2)$$

The time scale γ^{-1} is the ‘persistence’ time of a run that encodes the memory of the noise. In the limit $\gamma \rightarrow \infty$, $v_0 \rightarrow \infty$ but keeping the ratio $D_{\text{eff}} = v_0^2/2\gamma$ fixed, the noise $\xi(t)$ reduces to a white noise since

$$\langle \xi(t)\xi(t') \rangle = \frac{v_0^2}{\gamma} \left[\gamma e^{-2\gamma|t-t'|} \right] \rightarrow 2D_{\text{eff}} \delta(t-t'). \quad (3)$$

Thus in this so called ‘diffusive limit’, the persistent random walker $x(t)$ reduces to an ordinary Brownian motion. For finite γ (i.e., persistence time scale of memory), the RTP will be referred to as an ‘active’ particle. In the diffusive limit, the active particle dynamics reduces to an ordinary Brownian motion, which we refer to as a ‘passive’ motion.

Given the stochastic dynamics of the individual particles, starting from the step initial condition, our main object of interest is the flux Q_t of particles through the origin up to time t . If a trajectory crosses the origin from left to right, this will contribute a +1 to the net current while if it crosses from right to left, its contribution is -1. The flux Q_t is thus the net contribution to the current up to time t . Let us denote by $P(Q, t, \{x_i\})$ the probability distribution $\text{Prob.}(Q_t = Q)$ for a given initial condition where x_i ’s denote the initial positions of the particles at time $t = 0$. Following Derrida and Gerschenfeld, the effect of the initial condition on the distribution can be studied in two alternative ways, in analogy with the disordered systems where the realisation of a disorder plays an analogous role as the initial condition in our problem. It was indeed argued in [6] that one has to distinguish between two different ways of averaging over the initial conditions: (i) the annealed average, where the probability distribution of the flux is averaged over all the realizations of the initial condition and (ii) the quenched average where the probability distribution is computed for the *typical* initial configurations. Instead of considering the distribution $P(Q, t, \{x_i\})$ directly, it turns out to be convenient to consider its generating function $\langle e^{-pQ} \rangle_{\{x_i\}}$, where the angular brackets $\langle \dots \rangle_{\{x_i\}}$ denote an average over the history, but with fixed initial condition x_i . The annealed and quenched averages are now defined as follows:

$$\sum_{Q=0}^{\infty} e^{-pQ} P_{\text{an}}(Q, t) = \overline{\langle e^{-pQ} \rangle_{\{x_i\}}}, \quad (4)$$

$$\sum_{Q=0}^{\infty} e^{-pQ} P_{\text{qu}}(Q, t) = \exp \left[\overline{\ln \langle e^{-pQ} \rangle_{\{x_i\}}} \right], \quad (5)$$

where $\overline{\dots}$ denotes an average over the initial conditions. Note that in this problem Q_t is always an integer. As mentioned in the introduction, for the step initial condition, we can compute both $P_{\text{an}}(Q, t)$ and $P_{\text{qu}}(Q, t)$ (see Fig. 2 for a plot of these probability distributions) for arbitrary dynamics of the particles by using the identity $Q_t = N_t^+$, where N_t^+ is the number of particles on the right side of the origin at time t . Indeed, the only quantity that enters the computation for independent particles is the single particle Green’s function $G(x, x_0, t)$ denoting the probability density of finding the particle at position x at time t , starting from x_0 at $t = 0$. Let us first define a central object, that will appear in all our formulas

$$U(z, t) = \int_0^{\infty} G(x, -z, t) dx \quad , \quad z \geq 0, \quad (6)$$

obtained by integrating the Green’s function over the final position, with the initial position fixed at $x_0 = -z \leq 0$. If we can compute $U(z, t)$ for a given dynamics, we can express $P_{\text{an}}(Q, t)$ and $P_{\text{qu}}(Q, t)$ in terms of this central function $U(z, t)$. Our main results can now be summarised as follows.

Annealed case: In this case, we show that $P_{\text{an}}(Q, t)$ is always a Poisson distribution

$$P_{\text{an}}(Q = n, t) = e^{-\mu(t)} \frac{\mu(t)^n}{n!}, \quad n = 0, 1, 2, \dots, \quad (7)$$

where

$$\mu(t) = \rho \int_0^{\infty} dz U(z, t). \quad (8)$$

The mean and the variance of Q_t are both given by $\mu(t)$, which can be explicitly evaluated for different types of particle motion. For example, for a Brownian motion with diffusion constant D , using $G(x, x_0, t) = e^{-(x-x_0)^2/(4Dt)}/\sqrt{4\pi Dt}$

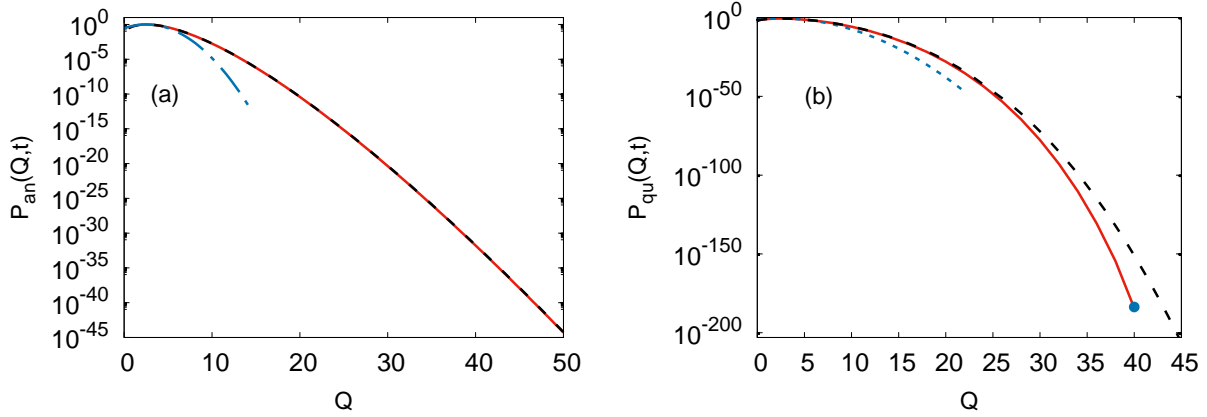


FIG. 2: (a) Annealed case: Semi-log plot of $P_{\text{an}}(Q, t)$ vs Q for RTPs (red solid line) using Eqs. (10), (12) and (13) compared to the diffusive case (black dashed curve) given by Eq. (12) with $\mu(t) = \rho\sqrt{\frac{Dt}{\pi}}$ for $\rho = 1$ and $t = 40$. For the RTP, we set $v_0 = \gamma = 1$, corresponding to an effective diffusion constant $D_{\text{eff}} = v_0^2/(2\gamma) = 1/2$, while we use, accordingly, $D = 1/2$ for diffusion. For such a (large) time where the scaling form (12) is expected to hold, the RTP and the diffusive cases are almost indistinguishable. Finally, the blue dashed curve corresponds to the typical Gaussian approximation with mean and variance $\mu(t)$ given in (10). (b) Quenched case: Semi-log plot of $P_{\text{qu}}(Q, t)$ vs Q for the same set of parameters for RTPs (red solid line), obtained from Eqs. (81) and (89), compared to the diffusive case (black dashed line) obtained from Eqs. (59) and (65). The blue dotted line corresponds to the Gaussian approximation with mean $\mu(t)$ given in (10) and variance given in (18). While the active and passive cases remain indistinguishable at small Q , the quenched distribution, at variance with the annealed one, carries a clear signature of activity at large Q . For example, in the quenched case, the maximum possible flux for the RTP is $Q = \rho v_0 t = 40$ (large blue dot).

in Eq. (6) we get

$$U(z, t) = \frac{1}{2} \operatorname{erfc} \left(\frac{z}{\sqrt{4Dt}} \right) \quad , \quad \text{and} \quad \mu(t) = \rho\sqrt{Dt/\pi} \quad , \quad (9)$$

where $\operatorname{erfc}(z) = (2/\sqrt{\pi}) \int_z^\infty e^{-u^2} du$. Our result for $P_{\text{an}}(Q = n, t)$ for the diffusive case is consistent with the result of Derrida and Gershenfeld [6] obtained by a different method.

In the case of the RTP dynamics, we find explicitly that at all t ,

$$\mu(t) = \frac{1}{2} \rho v_0 t e^{-\gamma t} [I_0(\gamma t) + I_1(\gamma t)] \quad , \quad (10)$$

where $I_0(z)$ and $I_1(z)$ are modified Bessel functions of the first kind. Its asymptotic behaviours are given by

$$\mu(t) \approx \begin{cases} \frac{\rho v_0}{2} t \quad , & \text{as } t \rightarrow 0 \quad , \\ \rho\sqrt{\frac{D_{\text{eff}} t}{\pi}} \quad , & \text{as } t \rightarrow \infty \quad , \end{cases} \quad (11)$$

where $D_{\text{eff}} = v_0^2/(2\gamma)$. Thus at late times, the RTP behaves like a diffusive particle with an effective diffusion constant D_{eff} .

Note that the Poisson distribution in Eq. (7) in the limit $Q \rightarrow \infty$, $\mu(t) \rightarrow \infty$, keeping the ratio $Q/\mu(t)$ fixed, can be written in a large deviation form (using simply Stirling's formula)

$$P_{\text{an}}(Q, t) \sim \exp \left[-\mu(t) \Psi_{\text{an}} \left(\frac{Q}{\mu(t)} \right) \right] \quad , \quad (12)$$

where the rate function $\Psi_{\text{an}}(q)$ is universal, i.e., independent of the particle dynamics, and is given by

$$\Psi_{\text{an}}(q) = q \ln q - q + 1 \quad , \quad q \geq 0 \quad . \quad (13)$$

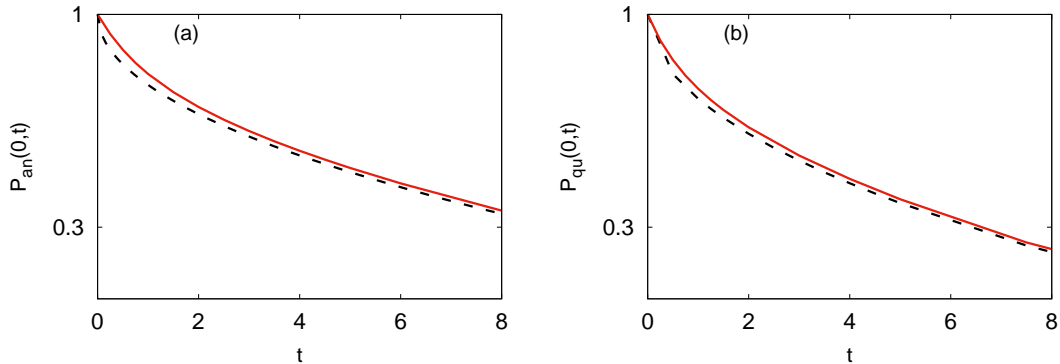


FIG. 3: (a) Semi-log plot of $P_{\text{an}}(Q=0, t) = e^{-\mu(t)}$ vs t for an RTP (red solid line) with $\mu(t)$ given in Eq. (15) compared to the diffusive case (black dashed line) corresponding to $\mu(t) = \rho\sqrt{\frac{Dt}{\pi}}$, for a density $\rho = 1$ in both cases. For the RTP, we set $v_0 = \gamma = 1$, corresponding to an effective diffusion constant $D_{\text{eff}} = v_0^2/(2\gamma) = 1/2$, while we set, accordingly, $D = 1/2$ in the case of diffusion. (b) Semi-log plot of $P_{\text{qu}}(Q=0, t)$ vs t as given in Eq. (19) both for RTPs (red solid line) using the result for $U(z, t)$ in (81) and for Brownian particles (black dashed line) for which $U(z, t)$ is given in (9). In both annealed and quenched cases, the zero-net flux probabilities for active and passive systems differ at short times but do coincide in the large time limit.

It has the asymptotic behaviours

$$\Psi_{\text{an}}(q) \approx \begin{cases} 1, & \text{as } q \rightarrow 0 \\ \frac{1}{2}(q-1)^2, & \text{as } q \rightarrow 1 \\ q \ln q, & \text{as } q \rightarrow \infty. \end{cases} \quad (14)$$

The quadratic behavior near the minimum at $q = 1$ indicates typical Gaussian fluctuations for Q , with mean and variance both equal to $\mu(t)$. Note that the dependence on the particle dynamics in Eq. (12) enters only through the parameter $\mu(t)$ but the function $\Psi_{\text{an}}(q)$ is universal.

We also note that, from our general result in Eq. (7), it follows that

$$\text{Prob.}(N_t^+ = 0) \Big|_{\text{an}} = P_{\text{an}}(Q=0, t) = e^{-\mu(t)}. \quad (15)$$

This result is valid for all t and gives the probability of the rare event that all the particles are back on the left side of the origin at time t , as discussed in the introduction. In Fig. 3 (a) we show a plot of $P_{\text{an}}(Q=0, t)$ as a function of time, both for RTP and for diffusive particles.

Quenched case: In this case, the generating function in Eq. (5), for arbitrary single particle dynamics, can again be expressed in terms of the central function $U(z, t)$ (6) as follows

$$\sum_{Q=0}^{\infty} P_{\text{qu}}(Q, t) e^{-pQ} = \exp \left[\rho \int_0^{\infty} dz \ln [1 - (1 - e^{-p})U(z, t)] \right]. \quad (16)$$

The quenched cumulants of Q can then be extracted and expressed in terms of $U(z, t)$. For instance, the quenched mean and the variance of Q are given by

$$\langle Q \rangle_{\text{qu}} = \rho \int_0^{\infty} U(z, t) dz, \quad (17)$$

$$\sigma_{\text{qu}}^2 = \langle Q^2 \rangle_{\text{qu}} - \langle Q \rangle_{\text{qu}}^2 = \rho \int_0^{\infty} U(z, t)(1 - U(z, t)) dz. \quad (18)$$

In addition, expanding the right hand side (rhs) in powers of e^{-p} and matching with the left hand side (lhs), one can in principle obtain $P_{\text{qu}}(Q, t)$ for any integer Q as a functional of $U(z, t)$. For example,

$$\text{Prob.}(N_t^+ = 0) \Big|_{\text{qu}} = P_{\text{qu}}(Q=0, t) = \exp \left[\rho \int_0^{\infty} \ln [1 - U(z, t)] dz \right], \quad (19)$$

which is valid for all times $t \geq 0$. However, the formula gets more complicated for higher values of Q . In Fig. 3 (b) we show a plot of $P_{\text{qu}}(Q = 0, t)$ as a function of time, both for RTP and for diffusive particles.

For the full quenched distribution, we first consider the diffusive motion of the particles. In this case, we obtain, in the scaling limit $Q \rightarrow \infty$, $t \rightarrow \infty$ keeping the ratio Q/\sqrt{t} fixed, the same large deviation form as Derrida and Gerschenfeld [6],

$$P_{\text{qu}}(Q, t) \sim \exp \left[-\rho\sqrt{Dt} \Psi_{\text{diff}} \left(\frac{Q}{\rho\sqrt{Dt}} \right) \right], \quad (20)$$

where the rate function $\Psi_{\text{diff}}(q)$ has the following precise asymptotics

$$\Psi_{\text{diff}}(q) \approx \begin{cases} \bar{\alpha} - q + q \ln(q/\bar{\beta}), & \text{as } q \rightarrow 0 \\ \sqrt{\frac{\pi}{2}} \left(q - \frac{1}{\sqrt{\pi}} \right)^2, & \text{as } q \rightarrow 1/\sqrt{\pi} \\ \frac{1}{12}q^3, & \text{as } q \rightarrow \infty, \end{cases} \quad (21)$$

with the two constants $\bar{\alpha}$ and $\bar{\beta}$ given explicitly by

$$\bar{\alpha} = -2 \int_0^\infty dz \ln \left(1 - \frac{1}{2} \text{erfc}(z) \right) = 0.675336 \dots \quad (22)$$

$$\bar{\beta} = \int_0^\infty dz \frac{\text{erfc}(z)}{1 - \frac{1}{2} \text{erfc}(z)} = 0.828581 \dots \quad (23)$$

Note that the large q behavior $\Psi_{\text{diff}}(q) \approx q^3/12$ coincides with the result of Derrida and Gerschenfeld [6] obtained by a different method. The small q behavior was not investigated in Ref. [6]. Taking the $q \rightarrow 0$ limit in Eq. (20) and using the small q behavior in the first line of Eq. (21) implies that for large t $P_{\text{qu}}(Q = 0, t) \sim \exp \left[-\bar{\alpha} \rho\sqrt{Dt} \right]$ where the constant $\bar{\alpha}$ is given in Eq. (22). In fact, this result is valid not just at large time but at all times. Indeed, substituting $U(z, t) = (1/2)\text{erfc}(z/\sqrt{4Dt})$ in our general formula (19), it follows that at all times $t \geq 0$,

$$P_{\text{qu}}(Q = 0, t) \Big|_{\text{diff}} = \exp \left[-\bar{\alpha} \rho\sqrt{Dt} \right]. \quad (24)$$

Interestingly, exactly the same rate function $\Psi_{\text{diff}}(q)$ also appeared in the completely different context, namely as a large deviation function characterising the distribution of the number of eigenvalues (in a disk of radius R) of a complex Ginibre ensemble of $N \times N$ Gaussian random matrices [36, 37].

We then consider the quenched flux distribution for the RTP dynamics. First, we show that, for small $Q \ll \sqrt{t}$, the flux distribution decays as a stretched exponential at late times, e. g. $P_{\text{qu}}(Q = 0, t)$ is given, for large t , by

$$P_{\text{qu}}(Q = 0, t) \Big|_{\text{RTP}} \sim \exp \left[-\bar{\alpha} \rho\sqrt{D_{\text{eff}} t} \right], \quad (25)$$

where $\bar{\alpha}$ is the same constant as in Eq. (22) and $D_{\text{eff}} = v_0^2/(2\gamma)$. One of the main results of this analysis is to find a new scaling limit $Q \rightarrow \infty$, $t \rightarrow \infty$, keeping the ratio $Q/(\rho v_0 t)$ fixed where the quenched distribution admits a large deviation form [quite different from the diffusive case in Eq. (20)]

$$P_{\text{qu}}(Q, t) \sim \exp \left[-\rho v_0 \gamma t^2 \Psi_{\text{RTP}} \left(\frac{Q}{\rho v_0 t} \right) \right], \quad (26)$$

where the rate function $\Psi_{\text{RTP}}(q)$ is given explicitly by

$$\Psi_{\text{RTP}}(q) = q - \frac{q}{2} \sqrt{1 - q^2} - \sin^{-1} \left[\sqrt{\frac{1 - \sqrt{1 - q^2}}{2}} \right], \quad 0 \leq q \leq 1. \quad (27)$$

The rate function has the asymptotic behavior

$$\Psi_{\text{RTP}}(q) \approx \begin{cases} \frac{q^3}{6}, & q \rightarrow 0 \\ 1 - \frac{\pi}{4}, & q = 1. \end{cases} \quad (28)$$

One consequence of our result is the prediction of the probability of the rare event that the flux Q up to time t achieves its maximum possible value, namely $Q = \rho v_0 t$ – this corresponds to the case where all the particles move ballistically to the right up to time t . We find that the probability of this rare event is given by

$$P_{\text{qu}}(Q = \rho v_0 t, t) \approx \exp \left[- \left(1 - \frac{\pi}{4} \right) \rho v_0 \gamma t^2 \right]. \quad (29)$$

Such a faster than exponential decay for the probability of this rare event is a nontrivial prediction of our theory.

III. THE GENERAL SETTING AND THE SINGLE-PARTICLE GREEN'S FUNCTION

We start with a step initial condition where N particles are initially located on the negative half line at positions $\{x_1, x_2, \dots, x_N\}$ where all $x_i < 0$. As stated before, for this step initial condition, the flux Q_t up to time t is identical in law to the number of particles N_t^+ to the right of the origin at time t . Let us introduce an indicator function $\mathcal{I}_i(t)$ such that $\mathcal{I}_i(t) = 1$ if the i th particle is to the right of the origin at time t , else $\mathcal{I}_i(t) = 0$. Hence we have

$$N_t^+ = \sum_{i=1}^N \mathcal{I}_i(t). \quad (30)$$

For fixed x_i 's the flux distribution is then given by

$$P(Q, t, \{x_i\}) = \text{Prob.}(N_t^+ = Q) = \left\langle \delta \left[Q - \sum_{i=1}^N \mathcal{I}_i(t) \right] \right\rangle_{\{x_i\}}, \quad (31)$$

where the angular brackets $\langle \dots \rangle_{\{x_i\}}$ denote an average over the history, but with fixed initial condition x_i . Taking the Laplace transform on both sides of Eq. (31) gives

$$\sum_{Q=0}^{\infty} e^{-pQ} P(Q, t, \{x_i\}) = \langle e^{-pQ} \rangle_{\{x_i\}} = \left\langle \exp \left[-p \sum_{i=1}^N \mathcal{I}_i(t) \right] \right\rangle_{\{x_i\}}. \quad (32)$$

Since the \mathcal{I}_i can only take the values 0 or 1, one has the identity $e^{-p\mathcal{I}_i} = 1 - (1 - e^{-p})\mathcal{I}_i$. Inserting this identity in Eq. (32) and using the independence of the random variables \mathcal{I}_i 's we get

$$\langle e^{-pQ} \rangle_{\{x_i\}} = \prod_{i=1}^N [1 - (1 - e^{-p}) \langle \mathcal{I}_i(t) \rangle_{\{x_i\}}], \quad (33)$$

where the right hand side (r.h.s.) implicitly depends on the x_i 's. The average $\langle \mathcal{I}_i(t) \rangle_{\{x_i\}}$ is just the probability that the i th particle is to the right of the origin at time t , starting initially at x_i and hence we have

$$\langle \mathcal{I}_i(t) \rangle_{\{x_i\}} = \int_0^{\infty} G(x, x_i, t) dx = U(-x_i, t), \quad x_i < 0, \quad (34)$$

where $G(x, x_i, t)$ is the single-particle Green's function, i.e., the propagator for a particle to reach x at time t , starting initially at $x_i < 0$. Note that $U(z, t)$ is defined in Eq. (6) and corresponds to the probability that a particle is on the positive side of the origin at time t , starting initially at $-z < 0$. Inserting Eq. (34) into Eq. (33), one obtains

$$\langle e^{-pQ} \rangle_{\{x_i\}} = \prod_{i=1}^N [1 - (1 - e^{-p})U(-x_i, t)], \quad x_i < 0, \quad \forall i = 1, \dots, N. \quad (35)$$

This Eq. (35) is general, i.e., valid for *any* set of non-interacting particles undergoing a common dynamics in one-dimension. The information about the dynamics is entirely encoded in the function $U(z, t)$.

For instance, for simple diffusion, the single-particle Green's function is given by

$$G(x, x_i, t) = \frac{1}{\sqrt{4\pi Dt}} \exp \left[-\frac{(x - x_i)^2}{4Dt} \right], \quad (36)$$

which gives $U(z, t) = (1/2)\text{erfc}(z/\sqrt{4Dt})$. For the RTP, on the other hand, the Green's function is known explicitly [15, 34]

$$G(x, x_i, t) = \frac{e^{-\gamma t}}{2} \left\{ \delta(x - x_i - v_0 t) + \delta(x - x_i + v_0 t) + \frac{\gamma}{v_0} \left[I_0(\omega) + \frac{\gamma t I_1(\omega)}{\rho} \right] \Theta(v_0 t - |x - x_i|) \right\}, \quad (37)$$

where ω is given by

$$\omega = \frac{\gamma}{v_0} \sqrt{v_0^2 t^2 - (x - x_i)^2}. \quad (38)$$

In Eq. (37), $\Theta(z)$ is the Heaviside Theta function, and $I_0(\omega)$ and $I_1(\omega)$ are modified Bessel functions. Computing $U(z, t) = \int_0^\infty G(x, -z, t) dx$ explicitly using Eq. (37) is complicated. It is however much more useful, as we will see later, to work with the Laplace transform of $G(x, x_i, t)$ with respect to t , which has a much simpler expression, namely

$$\tilde{G}(x, x_i, s) = \int_0^\infty dt e^{-st} G(x, x_i, t) = \frac{\lambda(s)}{2s} e^{\lambda(s)|x-x_i|}, \quad \lambda(s) = \frac{\sqrt{s(s+2\gamma)}}{v_0}. \quad (39)$$

The relation in Eq. (35) is the central result of this section and we will analyse the annealed and the quenched cases separately in the next two sections.

IV. FLUX DISTRIBUTION IN THE ANNEALED CASE

The annealed distribution $P_{\text{an}}(Q, t)$ is defined in Eq. (4) where the $\overline{\dots}$ denotes an average over the initial conditions. Performing this average in Eq. (35) gives

$$\overline{\langle e^{-pQ} \rangle_{\{x_i\}}} = \prod_{i=1}^N \left[1 - (1 - e^{-p}) \overline{U(-x_i, t)} \right], \quad (40)$$

where $U(-x_i, t)$ is defined in Eq. (34). To perform the average over the initial conditions with a fixed uniform density ρ , we assume that each of the N particles is distributed independently and uniformly over a box $[-L, 0]$ and then eventually take the limit $N \rightarrow \infty$, $L \rightarrow \infty$ keeping the density $\rho = N/L$ fixed. For this uniform measure, each x_i is uniformly distributed in the box $[-L, 0]$. Using the independence of the x_i 's we then get

$$\overline{\langle e^{-pQ} \rangle_{\{x_i\}}} = \prod_{i=1}^N \left[1 - (1 - e^{-p}) \int_{-L}^0 U(-x_i, t) \frac{dx_i}{L} \right] = \left[1 - \frac{1}{L} (1 - e^{-p}) \int_0^L U(z, t) dz \right]^N, \quad (41)$$

where, in the last equality, we made the change of variable $z = -x_i$. Taking now the limit $N \rightarrow \infty$, $L \rightarrow \infty$ keeping $\rho = N/L$ fixed gives

$$\sum_{Q=0}^{\infty} e^{-pQ} P_{\text{an}}(Q, t) = \overline{\langle e^{-pQ} \rangle_{\{x_i\}}} = \exp[-\mu(t) (1 - e^{-p})], \quad \text{where} \quad \mu(t) = \rho \int_0^\infty dz U(z, t). \quad (42)$$

By expanding $\exp[-\mu(t) (1 - e^{-p})]$ in powers of e^{-p} and comparing to the left hand side, we see that Q can take only integer values $Q = n = 0, 1, 2, \dots$ and the probability distribution is simply a Poisson distribution with mean $\mu(t)$ as given in Eqs. (7) and (8).

This Poisson distribution, in the annealed case, is thus universal, i.e., holds for any dynamics. The details of the dynamics is encoded in the single parameter $\mu(t)$ which can be computed explicitly for different types of dynamics. For example, for diffusing particles, using the explicit expression for the Brownian propagator, we get $U(z, t) = (1/2)\text{erfc}(z/\sqrt{4Dt})$ and, hence, $\mu(t) = \rho\sqrt{Dt/\pi}$ as mentioned in Eq. (9). In contrast, for the RTP dynamics, $\mu(t)$ is nontrivial. As discussed earlier, computing $U(z, t)$ from the Green's function in Eq. (37) is difficult. Consequently, calculating $\mu(t) = \rho \int_0^\infty U(z, t) dz$ is also hard. However, it turns out that its Laplace transform is much easier to manipulate, due to the simple nature of the formula in Eq. (39). The Laplace transform of $\mu(t)$ is given by

$$\tilde{\mu}(s) = \int_0^\infty dt e^{-st} \mu(t) = \rho \int_0^\infty dz \tilde{U}(z, s), \quad \text{with} \quad \tilde{U}(z, s) = \int_0^\infty dt e^{-st} U(z, t), \quad (43)$$

where we have used the relation $\mu(t) = \rho \int_0^\infty U(z, t) dz$. The Laplace transform of $U(z, t)$ can be computed as follows

$$\tilde{U}(z, s) = \int_0^\infty dt e^{-st} U(z, t) = \int_0^\infty dt e^{-st} \int_0^\infty G(x, -z, t) dx . \quad (44)$$

Exchanging the integrals over x and t , and using the relation in Eq. (39) and integrating over x we get

$$\tilde{U}(z, s) = \frac{e^{-\lambda(s)z}}{2s} , \quad \text{where} \quad \lambda(s) = \frac{\sqrt{s(s+2\gamma)}}{v_0} . \quad (45)$$

Inserting this relation in Eq. (43) and performing the integral over z , we get

$$\tilde{\mu}(s) = \frac{1}{2s\lambda(s)} = \frac{v_0}{2s\sqrt{s(s+2\gamma)}} . \quad (46)$$

This Laplace transform can be explicitly inverted, yielding the result in Eq. (10).

V. FLUX DISTRIBUTION IN THE QUENCHED CASE

As stated in Section II, the quenched flux distribution is defined as

$$\sum_{Q=0}^{\infty} P_{\text{qu}}(Q, t) e^{-pQ} = \exp \left[\overline{\ln [\langle e^{-pQ} \rangle_{\{x_i\}}]} \right] , \quad (47)$$

where $\overline{\dots}$ once again represents an average over the initial positions $\{x_i\}$. Our starting point is again Eq. (35). Taking the logarithm on both sides of (35) gives

$$\ln [\langle e^{-pQ} \rangle_{\{x_i\}}] = \sum_{i=1}^N \ln [1 - (1 - e^{-p})U(-x_i, t)] . \quad (48)$$

We now perform the average over the initial positions, as in the annealed case, i.e., choosing each x_i independently and uniformly from the box $[-L, 0]$ and finally taking the limit $N \rightarrow \infty$, $L \rightarrow \infty$ keeping $\rho = N/L$ fixed. This gives

$$\overline{\ln [\langle e^{-pQ} \rangle_{\{x_i\}}]} = \frac{N}{L} \int_{-L}^0 dx_i \ln [1 - (1 - e^{-p})U(-x_i, t)] \longrightarrow \rho \int_0^\infty dz \ln [1 - (1 - e^{-p})U(z, t)] . \quad (49)$$

Therefore the Laplace transform of the quenched flux distribution is given by

$$\sum_{Q=0}^{\infty} P_{\text{qu}}(Q, t) e^{-pQ} = \exp [I(p, t)] , \quad (50)$$

where

$$I(p, t) = \rho \int_0^\infty dz \ln [1 - (1 - e^{-p})U(z, t)] . \quad (51)$$

Before extracting the full distribution $P_{\text{qu}}(Q, t)$ from this Laplace transform, it is useful to study first the asymptotic behaviors of $I(p, t)$ in the two limits : (i) $p \rightarrow 0$ and (ii) $p \rightarrow \infty$.

- $p \rightarrow 0$ limit: Expanding e^{-p} in powers of p in Eq. (51), we get

$$I(p, t) = -p \rho \int_0^\infty dz U(z, t) + \frac{p^2}{2} \rho \int_0^\infty dz U(z, t) [1 - U(z, t)] + \mathcal{O}(p^3) . \quad (52)$$

Substituting this in Eq. (50) and expanding both sides in powers of p we immediately get the mean and the variance of the flux Q_t for the quenched case as stated in Eqs. (17) and (18) respectively.

- $p \rightarrow \infty$ limit: In this case we expand $I(p, t)$ in Eq. (51) in powers of e^{-p} . The two leading terms are given by

$$I(p, t) = A(t) + B(t)e^{-p} + \mathcal{O}(e^{-2p}), \quad (53)$$

where

$$A(t) = \rho \int_0^\infty \ln[1 - U(z, t)] dz \quad (54)$$

$$B(t) = \rho \int_0^\infty \frac{U(z, t)}{1 - U(z, t)} dz. \quad (55)$$

Substituting this expansion (53) on the rhs of Eq. (50) and matching the powers of e^{-p} on both sides of Eq. (50) immediately gives

$$P_{\text{qu}}(Q = 0, t) = e^{A(t)} = \exp \left[\rho \int_0^\infty \ln(1 - U(z, t)) dz \right] \quad (56)$$

$$P_{\text{qu}}(Q = 1, t) = B(t) e^{A(t)}. \quad (57)$$

The first line yields the general result mentioned in Eq. (19).

These results so far are quite general, i.e., they hold for any dynamics – the dependence on the dynamics comes only through the function $U(z, t)$. In the following, we focus on two interesting dynamics, namely the diffusive and the RTP and extract the large time behavior of $P_{\text{qu}}(Q, t)$ using Eqs. (50) and (51).

A. $P_{\text{qu}}(Q, t)$ for simple diffusion

In this case, using the explicit expression $U(z, t) = (1/2)\text{erfc}(z/\sqrt{4Dt})$, we get from Eq. (51)

$$I(p, t) = \rho\sqrt{4Dt} \int_0^\infty dz \ln \left[1 - \frac{1}{2}(1 - e^{-p})\text{erfc}(z) \right] = -\rho\sqrt{Dt} \phi(p), \quad (58)$$

where

$$\phi(p) = -2 \int_0^\infty dz \ln \left[1 - \frac{1}{2}(1 - e^{-p})\text{erfc}(z) \right]. \quad (59)$$

Therefore Eq. (50) reads for all time t

$$\sum_{Q=0}^{\infty} e^{-pQ} P_{\text{qu}}(Q, t) = \exp \left[-\rho\sqrt{Dt} \phi(p) \right]. \quad (60)$$

In the long time limit $t \rightarrow \infty$, we anticipate, and verify a posteriori, that $P_{\text{qu}}(Q, t)$ takes a large deviation form in the limit where $Q \rightarrow \infty$, $t \rightarrow \infty$ but with the dimensionless ratio $q = Q/(\rho\sqrt{Dt})$ fixed

$$P_{\text{qu}}(Q, t) \sim \exp \left[-\rho\sqrt{Dt} \Psi_{\text{diff}} \left(\frac{Q}{\rho\sqrt{Dt}} \right) \right], \quad (61)$$

where $\Psi_{\text{diff}}(q)$ is a rate function that we wish to compute. Substituting this large deviation form (61) on the left hand side (lhs) of Eq. (60) and replacing the discrete sum over Q by an integral (which is valid for large $Q \sim \sqrt{t}$), we get

$$\int_0^\infty e^{-pQ} P_{\text{qu}}(Q, t) dQ \sim \rho\sqrt{Dt} \int_0^\infty e^{-\rho\sqrt{Dt} [pq + \Psi_{\text{diff}}(q)]} dq. \quad (62)$$

For large t , we can now evaluate the integral over q in Eq. (62) by a saddle point method, which gives

$$\int_0^\infty e^{-pQ} P_{\text{qu}}(Q, t) dQ \sim \exp \left[-\rho\sqrt{Dt} \min_q [pq + \Psi_{\text{diff}}(q)] \right]. \quad (63)$$

Comparing this with the rhs of Eq. (60) we get

$$\min_q [p q + \Psi_{\text{diff}}(q)] = \phi(p) . \quad (64)$$

Inverting this Legendre transform one gets

$$\Psi_{\text{diff}}(q) = \max_p [\phi(p) - p q] , \quad (65)$$

where $\phi(p)$ is given in Eq. (59).

Knowing $\phi(p)$ explicitly, one can plot the large deviation function $\Psi_{\text{diff}}(q)$ using Eq. (65) – see Fig. 4. Clearly, $\Psi_{\text{diff}}(q)$ has a concave shape with a minimum at $q = q_{\text{min}}$, the value of q_{min} will be computed shortly. The asymptotic behaviors of the rate function $\Psi_{\text{diff}}(q)$ can also be extracted in the limits $q \rightarrow q_{\text{min}}$, $q \rightarrow 0$ and $q \rightarrow \infty$ by analysing $\phi(p)$ respectively in the limits $p \rightarrow 0$, $p \rightarrow +\infty$ and $p \rightarrow -\infty$ (where $\phi(p)$ in Eq. (59) has to be continued analytically to negative p). The results are summarised in Eqs. (21), (22) and (23) in section II. Below we provide the derivation of these results.

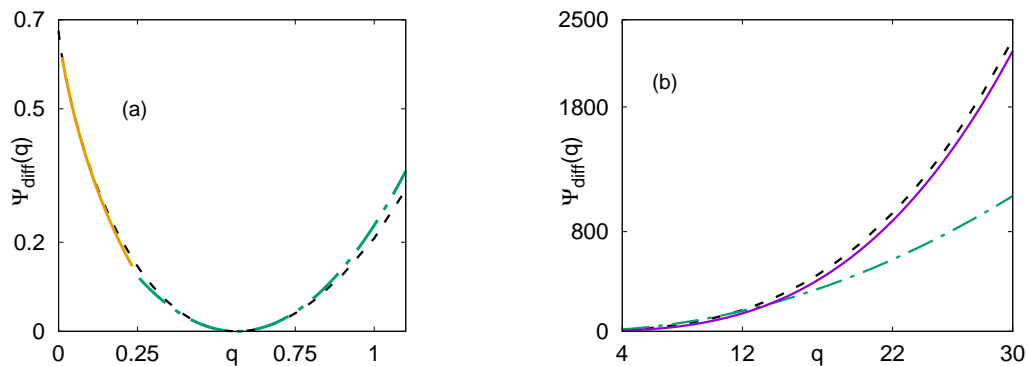


FIG. 4: Large deviation function $\Psi_{\text{diff}}(q)$ vs q for the diffusive case with quenched initial conditions. On both panels, the dashed black lines correspond to evaluating via Mathematica $\Psi_{\text{diff}}(q)$ from Eq. (65) with $\phi(p)$ given in Eq. (59). On the left panel (a), the solid yellow curve corresponds to the small q asymptotic behavior of $\Psi_{\text{diff}}(q)$ in Eq. (76) and the dashed-dotted green curve corresponds to the quadratic behavior in Eq. (69). On the right panel (b), we zoom in on the large q tail. The solid violet curve corresponds to the leading asymptotic behavior $\Psi_{\text{diff}}(q) \approx q^3/12$, while the dashed-dotted green curve is the quadratic behavior as in Eq. (69). The violet and the green curves clearly demonstrate the non-Gaussian tail of $\Psi_{\text{diff}}(q)$.

1. Typical Fluctuations : $Q \sim \langle Q \rangle_{\text{qu}}$

In order to derive the result for $\Psi_{\text{diff}}(q \rightarrow q_{\text{min}})$, we need to analyze $\phi(p)$ for $p \rightarrow 0$. We expand $\phi(p)$ in Eq. (59) up to order p^2 and get

$$\phi(p) = \alpha p - \beta p^2 + \mathcal{O}(p^3) , \quad (66)$$

where

$$\alpha = \int_0^\infty \text{erfc}(z) dz = \sqrt{\frac{1}{\pi}} \quad (67)$$

$$\beta = \frac{1}{4} \int_0^\infty (2 \text{erfc}(z) - \text{erfc}^2(z)) dz = \frac{1}{\sqrt{8\pi}} . \quad (68)$$

Substituting $\phi(p) = \alpha p - \beta p^2$ in Eq. (65) and maximising with respect to p gives a quadratic form for the rate function

$$\Psi_{\text{diff}}(q) \sim \frac{(q - \alpha)^2}{4\beta} = \sqrt{\frac{\pi}{2}} \left(q - \sqrt{\frac{1}{\pi}} \right)^2 . \quad (69)$$

This form holds for q close to $q_{\min} = \alpha = 1/\sqrt{\pi}$ and gives the result in the second line in Eq. (21). Substituting this quadratic behavior in the large deviation form in Eq. (61) predicts a Gaussian form for the quenched flux distribution for q close to q_{\min}

$$P_{\text{qu}}(Q, t) \sim \exp \left[-\frac{(Q - \langle Q \rangle_{\text{qu}})^2}{2\sigma_{\text{qu}}^2} \right] \quad (70)$$

where the mean and the variance are given by

$$\langle Q \rangle_{\text{qu}} = \rho \sqrt{\frac{Dt}{\pi}} \quad (71)$$

$$\sigma_{\text{qu}}^2 = \rho \sqrt{\frac{Dt}{2\pi}}. \quad (72)$$

Notice that these expressions for the mean and the variance, though derived here for large t , actually hold for all t , as one can verify directly from the formulae in Eqs. (17) and (18) with $U(z, t) = (1/2)\text{erfc}(z/\sqrt{4Dt})$. Comparing with the annealed case, while the means in both cases are identical, both given by $\mu(t) = \rho\sqrt{Dt/\pi}$, their variances and higher moments differ. For example, the variance in the annealed case is $\mu(t) = \rho\sqrt{Dt/\pi}$ which differs by a factor $1/\sqrt{2}$ from the quenched case in Eq. (72). These results agree with those obtained in [6]. This typical quadratic behavior is shown by the dashed-dotted green curve in Fig. 4.

2. Atypical fluctuations on the left of the mean: $Q \ll \langle Q \rangle_{\text{qu}}$

In order to infer about the fluctuations of $P_{\text{qu}}(Q, t)$ around $Q \rightarrow 0$, we need to evaluate how $\Psi_{\text{diff}}(q)$ behaves when $q \rightarrow 0$. This corresponds to the limit $p \rightarrow \infty$ for $\phi(p)$ from Eq. (65). We use the large p expansion in Eq. 53, and evaluate $A(t)$ and $B(t)$ from Eq. (54) using $U(z, t) = (1/2)\text{erfc}(z/\sqrt{4Dt})$. This gives

$$A(t) = -\bar{\alpha} \rho \sqrt{4Dt}, \quad \text{where } \bar{\alpha} = -2 \int_0^\infty \ln \left[1 - \frac{1}{2} \text{erfc}(z) \right] dz = 0.675336 \dots \quad (73)$$

$$B(t) = \bar{\beta} \rho \sqrt{4Dt}, \quad \text{where } \bar{\beta} = \int_0^\infty \frac{\text{erfc}(z)}{1 - \frac{1}{2} \text{erfc}(z)} dz = 0.828582 \dots \quad (74)$$

From Eqs. (58) and (59) we get the two leading terms of $\phi(p)$ for large $p > 0$

$$\phi(p) = -\frac{I(p, t)}{\rho\sqrt{Dt}} \approx \bar{\alpha} - \bar{\beta} e^{-p}. \quad (75)$$

Plugging this result for $\phi(p)$ in Eq. (65) and maximizing with respect to p , we get the leading small q behavior of $\Psi_{\text{diff}}(q)$

$$\Psi_{\text{diff}}(q) \approx \bar{\alpha} - q + q \ln \left(\frac{q}{\bar{\beta}} \right). \quad (76)$$

This reproduces the first line of Eq. (21). In particular, for $q = 0$, using $\Psi_{\text{diff}}(q = 0) = \bar{\alpha}$ in Eq. (61), we obtain $P_{\text{qu}}(Q = 0, t) \sim \exp(-\bar{\alpha} \rho \sqrt{Dt})$ as announced in Eq. (24). The small q behavior of $\Psi_{\text{diff}}(q)$ is shown by the solid yellow curve in Fig. 4(a).

3. Atypical fluctuations on the right of the mean: $Q \gg \langle Q \rangle_{\text{qu}}$

In order to derive the large q asymptotics of $\Psi_{\text{diff}}(q)$ from Eq. (65), we first need to continue $\phi(p)$ in Eq. (59) analytically to negative p and use its asymptotics in the limit $p \rightarrow -\infty$. For this, it is convenient to write first $p = -u$ where $u = |p|$. We write

$$\phi(p = -u) = \tilde{\phi}(u) = -2 \int_0^\infty dz \ln \left[1 + \frac{(e^u - 1)}{2} \text{erfc}(z) \right] \underset{u \rightarrow \infty}{\approx} -2 \int_0^\infty dz \ln \left[1 + \frac{e^u}{2} \text{erfc}(z) \right]. \quad (77)$$

To extract the large u behavior of $\tilde{\phi}(u)$ from the integral on the rhs, it is convenient to take the derivative with respect to u

$$\tilde{\phi}'(u) \approx -2 \int_0^\infty dz \frac{\frac{e^u}{2} \operatorname{erfc}(z)}{1 + \frac{e^u}{2} \operatorname{erfc}(z)}. \quad (78)$$

For large u the dominant contribution to this integral comes from large z where $\operatorname{erfc}(z) \approx e^{-z^2}/(z\sqrt{\pi})$. Hence we see that, for $z > \sqrt{u}$ the integrand is essentially 0 as $u \rightarrow \infty$, while, for $z < \sqrt{u}$, the integrand is 1 as $u \rightarrow \infty$. Hence, the integrand can be approximated by a Fermi function

$$\tilde{\phi}'(u) \approx -2 \int_0^{\sqrt{u}} dz = -2\sqrt{u}. \quad (79)$$

Integrating it back, we get the leading order behavior for $\tilde{\phi}(u)$ for large u

$$\tilde{\phi}(u) \approx -\frac{4}{3}u^{\frac{3}{2}}. \quad (80)$$

Therefore $\phi(p) \approx -(4/3)(-p)^{3/2}$ as $p \rightarrow -\infty$. Substituting this behavior in Eq. (65) and maximizing with respect to p one gets $\Psi_{\text{diff}}(q) \approx q^3/12$ as $q \rightarrow \infty$. This then gives the last line of the result in Eq. (21). As mentioned earlier, this leading large q asymptotic behavior of $\Psi_{\text{diff}}(q)$ coincides with the result of Ref. [6] obtained by a different method. The large q behavior of $\Psi_{\text{diff}}(q)$ is shown solid the solid violet curve in Fig. 4(b).

B. $P_{\text{qu}}(Q, t)$ for run-and-tumble particles

In this case, our starting point again are Eqs. (50) and (51), except that the function $U(z, t)$ for the RTP is more complicated. Its Laplace transform is given in Eq. (45). As shown in Appendix C of [32] it can be formally inverted to obtain $U(z, t)$ in real time

$$U(z, t) = \frac{1}{2} \left[e^{\frac{-\gamma z}{v_0}} + \frac{\gamma z}{v_0} \int_1^{\frac{v_0 t}{z}} dT \frac{e^{\frac{-\gamma z T}{v_0}} I_1\left(\frac{\gamma z}{v_0} \sqrt{T^2 - 1}\right)}{\sqrt{T^2 - 1}} \right] \Theta(v_0 t - z). \quad (81)$$

However, it turns out that this expression is not very useful to extract the large deviation function at late times.

Before proceeding to compute the large deviation function at late times, it is useful to discuss the large t behavior of $P_{\text{qu}}(Q, t)$ in different regimes of Q . In the following, we will first discuss the $Q \rightarrow 0$ limit of $P_{\text{qu}}(Q, t)$, followed by the discussion of the typical fluctuations where $Q = \mathcal{O}(\sqrt{t})$. In this regime, we will recover the Gaussian fluctuations. When $Q/(\rho\sqrt{Dt}) \gg 1$, we expect to recover the large deviation regime for the diffusive behaviour discussed in the previous section. This is because, as explained in the introduction, at late times, the RTP motion essentially reduces to that of a diffusive particle with an effective diffusion constant $D_{\text{eff}} = v_0^2/(2\gamma)$. However, there exists yet another ‘‘larger deviations regime’’ where $Q \sim \mathcal{O}(t)$ where we will show that $P_{\text{qu}}(Q, t)$ carries the signature of activity and has a novel large deviation form

$$P_{\text{qu}}(Q, t) \sim \exp \left[-\rho v_0 \gamma t^2 \Psi_{\text{RTP}} \left(\frac{Q}{\rho v_0 t} \right) \right]. \quad (82)$$

In the following, we will indeed compute this rate function $\Psi_{\text{RTP}}(q)$ and show that it is given by Eq. (27).

1. Typical fluctuations: $Q \sim \langle Q \rangle_{\text{qu}}$

In order to extract the typical fluctuations of Q_t around its mean value for the RTP case, we need to use the small p expansion of $I(p, t)$ in Eq. (50). Quite generally, the small p expansion of $I(p, t)$ is given in Eq. (52). We use this expansion on the rhs of Eq. (50) and approximate the sum on lhs by an integral. The resulting Laplace transform can be easily inverted and yields a Gaussian form

$$P_{\text{qu}}(Q, t) \approx \exp \left[-\frac{(Q - \langle Q \rangle_{\text{qu}})^2}{2\sigma_{\text{qu}}^2} \right], \quad (83)$$

where $\langle Q \rangle_{\text{qu}}$ and σ_{qu}^2 are given in Eqs. (17) and (18) respectively where $U(z, t)$ is given in Eq. (81) – alternatively its Laplace transform is given by the simpler form in Eq. (45). The mean value $\langle Q \rangle_{\text{qu}}$ can be computed explicitly. Indeed

$$\langle Q \rangle_{\text{qu}} = \rho \int_0^\infty U(z, t) dz = \mu(t) = \frac{\rho v_0}{2} t e^{-\gamma t} [I_0(\gamma t) + I_1(\gamma t)] , \quad (84)$$

where the last equality follows from Eq. (10). The variance $\sigma_{\text{qu}}^2 = \rho \int_0^\infty U(z, t) [1 - U(z, t)] dz$ is however difficult to compute explicitly using $U(z, t)$ from Eq. (81). However, it can be easily evaluated numerically. At large times, $\langle Q \rangle_{\text{qu}}$ and σ_{qu}^2 converge to the diffusive limits given in Eqs. (71) and (72) respectively.

2. Atypical fluctuations on the left of the mean: $Q \ll \langle Q \rangle_{\text{qu}}$

Exactly at $Q = 0$ or $Q = 1$, we have an exact expression at all times t for $P_{\text{qu}}(Q, t)$ in terms of $U(z, t)$, as given in Eqs. (56) and (57). The function $U(z, t)$ for RTP appearing in these expressions is given in Eq. (81). Given this rather complicated expression of $U(z, t)$, it is hard to obtain explicit formulae valid at all times for $P_{\text{qu}}(Q, t)$ even for $Q = 0$ or $Q = 1$. However, at late times, since $U(z, t)$ converges at late times to that of the diffusive limit in Eq. (9) with an effective diffusion constant $D_{\text{eff}} = v_0^2/(2\gamma)$, we recover the diffusive results for this extreme left tail of $P_{\text{qu}}(Q, t)$. For instance $P_{\text{qu}}(Q = 0, t)$, which represents the probability of having no particle on the right side of the origin at time t , decays at late times as in the diffusive case

$$P_{\text{qu}}(Q = 0, t) \Big|_{\text{RTP}} \approx \exp \left[-\bar{\alpha} \rho \sqrt{D_{\text{eff}} t} \right] , \quad (85)$$

where $\bar{\alpha} = 0.675336 \dots$ is given in Eq. (22).

3. Atypical fluctuations on the right of the mean: $Q \sim \mathcal{O}(t) \gg \langle Q \rangle_{\text{qu}}$

In this section, we derive the result in Eq. (82). We recall that in the diffusive case, the atypical fluctuations of Q are encoded in the large deviation form in Eq. (61) with $Q \sim \rho \sqrt{Dt}$. The extreme fluctuations to the right of $\langle Q \rangle_{\text{qu}}$ in this case are described by the large argument behavior of the large deviation function $\Psi_{\text{diff}}(q = Q/(\rho \sqrt{Dt}))$, i.e., when $Q \gg \rho \sqrt{Dt}$. Thus, in the diffusive case, there is a single scale for the fluctuations of Q at late times, namely $Q \sim \sqrt{t}$. In contrast, for the RTP, in addition to the scale \sqrt{t} that describes the moderate large deviations around the mean, there is yet another scale where $Q \sim t$. This comes from the fact that each particle in time t can move a maximum distance $v_0 t$, where v_0 is the velocity. So for an initial density ρ , the maximum possible flux through the origin is $Q_{\text{max}} = \rho v_0 t$. Hence $Q \sim t$ describes the scale of fluctuations at the very right tail of the distribution $P_{\text{qu}}(Q, t)$.

To extract this extreme right tail, we again start from Eqs. (50) and (51) with $U(z, t)$, for RTP, given by its Laplace transform in Eq. (45). Before extracting the large deviation form of $P_{\text{qu}}(Q, t)$, we first analyse $U(z, t)$ in the limit $z \sim t$. Inverting the Laplace transform of $U(z, t)$ in Eq. (45) we get

$$U(z, t) = \int_{\Gamma} \frac{ds}{2\pi i} \exp \left[t \left(s - \sqrt{s(s+2\gamma)} \frac{z}{v_0 t} \right) \right] , \quad (86)$$

where Γ represents the Bromwich contour in the complex s -plane. In the limit $t \rightarrow \infty$, $z \rightarrow \infty$ with the ratio z/t fixed, the integral can be evaluated by the saddle-point method, which yields (up to pre-exponential factors)

$$U(z, t) \approx \exp \left[-\gamma t \left(1 - \sqrt{1 - \frac{z^2}{v_0^2 t^2}} \right) \right] \Theta(v_0 t - z) . \quad (87)$$

We have checked numerically that this approximation (87) works very well, at large times, as one would expect.

To extract the large $Q \sim t \gg \langle Q \rangle_{\text{qu}}$ behavior from Eq. (50) we need to analytically continue $I(p, t)$ to p negative and study the limit $p \rightarrow -\infty$, as in the diffusive case. Setting $p = -u$ with $u > 0$, and approximating the discrete sum on the lhs of Eq. (50) by an integral, we get

$$\int_0^\infty P_{\text{qu}}(Q, t) e^{uQ} dQ \approx e^{\tilde{I}(u, t)} , \quad (88)$$

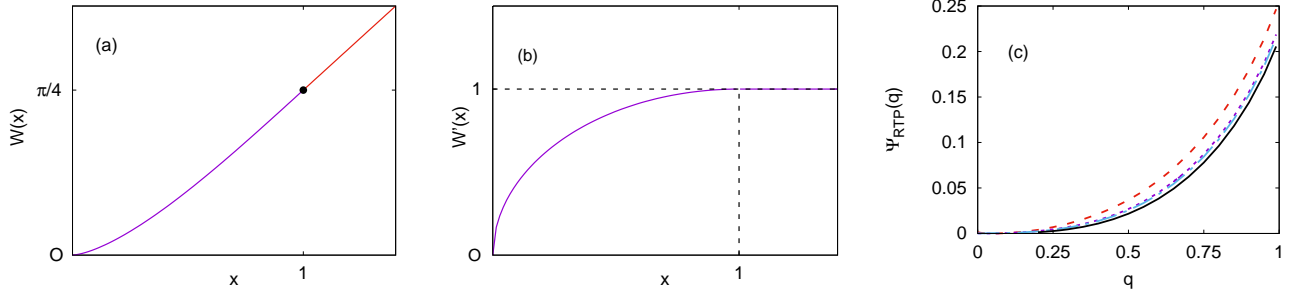


FIG. 5: (a) Plot of $W(x)$ vs x with $W(x)$ given by Eq. (97). The non-analytical point at $x = 1$ is shown by a black dot where $W(x)$ and its first two derivatives are continuous, while the third derivative is discontinuous, as in Eq. (98). (b) Plot of $W'(x)$ vs x where $W'(x)$ can be read off from Eq. (96). Note that $W'(x) < 1$ for $x < 1$ and saturates at 1 at $x = 1$. (c) Large deviation function $\psi_{\text{RTP}}(q)$ vs q for the run-and-tumble case. Black solid line represents the analytical expression given in Eq. (27) valid at very large time. Dashed lines ($t = 100$ (red-dashed), $t = 400$ (violet-dotted) and $t = 600$ (blue dashed-dotted)) correspond to the finite time evaluation of $\max_x \left[\frac{qu}{\gamma t} - \frac{\tilde{I}(u,t)}{\rho v_0 \gamma t^2} \right]$ using Eq. (89) – together with Eq. (89) with $\rho = v_0 = 1, \gamma = 0.5$ – with Mathematica.

where

$$\tilde{I}(u, t) = \rho \int_0^\infty dz \ln(1 + (e^u - 1)U(z, t)) \underset{u \rightarrow \infty}{\approx} \rho \int_0^\infty dz \ln(1 + e^u U(z, t)). \quad (89)$$

To extract the large u behavior of $\tilde{I}(u, t)$ we follow the same procedure as in the diffusive case and take a derivative with respect to u . We get

$$\frac{d\tilde{I}(u, t)}{du} \approx \rho \int_0^\infty \frac{dz}{1 + e^{-u} \frac{1}{U(z, t)}}. \quad (90)$$

For large u , this integral is dominated by the region where $z \sim t$ where we can use the approximate form of $U(z, t)$ given in Eq. (87). Substituting this form for $U(z, t)$ in Eq. (90), we get

$$\frac{d\tilde{I}(u, t)}{du} \approx \rho \int_0^{v_0 t} \frac{dz}{1 + \exp \left[- \left(u - \gamma t + \gamma t \sqrt{1 - \frac{z^2}{v_0^2 t^2}} \right) \right]}. \quad (91)$$

We now analyse this integral in two different cases, assuming $u \sim t \gg 1$:

- If $u > \gamma t$: in this case as $t \rightarrow \infty$ it is clear that the integrand in Eq. (91) is always 1 for any z . Hence

$$\frac{d\tilde{I}(u, t)}{du} \approx \rho v_0 t \quad \text{if } u > \gamma t. \quad (92)$$

- If $u < \gamma t$: this case is a bit more complicated to analyze. Since $u < \gamma t$ the argument of the exponential in Eq. (91) can be either positive or negative. Accordingly, the integrand will either 0 or 1 for large $u \sim t \gg 1$. The value of z for which the argument of the exponential changes sign is given by

$$z^*(u) = \frac{v_0}{\gamma} \sqrt{u(2\gamma t - u)}. \quad (93)$$

Thus, if $z > z^*(u)$ the integrand is 0 while for $z < z^*(u)$ the integrand is 1. Hence this integral over z in (91) gets cut-off at $z = z^*(u)$ (note that $z^*(u) < v_0 t$ for all u). Hence we get

$$\frac{d\tilde{I}(u, t)}{du} \approx \rho z^*(u) = \rho \frac{v_0}{\gamma} \sqrt{u(2\gamma t - u)} \quad \text{if } u < \gamma t. \quad (94)$$

Integrating it back with respect to u we obtain

$$\tilde{I}(u, t) \approx \rho v_0 \gamma t^2 W \left(\frac{u}{\gamma t} \right) \quad (95)$$

where

$$W(x) = \begin{cases} \int_0^x \sqrt{y(2-y)} dy & , \quad \text{if } x < 1 , \\ \int_0^1 \sqrt{y(2-y)} dy + (x-1) & , \quad \text{if } x > 1 . \end{cases} \quad (96)$$

Performing these integrals explicitly, we get

$$W(x) = \begin{cases} \frac{(x-1)}{2} \sqrt{x(2-x)} + \sin^{-1}(\sqrt{x/2}) & , \quad x < 1 \\ \frac{\pi}{4} + x - 1 & , \quad x > 1 . \end{cases} \quad (97)$$

The function $W(x)$ is plotted vs x in Fig. 5 (a). Interestingly, while $W(x)$ and its first two derivatives are continuous at $x = 1$, its third derivative is discontinuous. Indeed one has

$$\begin{aligned} W'''(x \rightarrow 1^-) &= -1 \\ W'''(x \rightarrow 1^+) &= 0 . \end{aligned} \quad (98)$$

Using this result for $W(x)$ in Eq. (97) gives us an expression for $\tilde{I}(u, t)$ in (95). We then substitute this expression for $\tilde{I}(u, t)$ in Eq. (88) to get

$$\int_0^\infty P_{\text{qu}}(Q, t) e^{uQ} dQ \sim \exp \left[\rho v_0 \gamma t^2 W \left(\frac{u}{\gamma t} \right) \right] . \quad (99)$$

Inverting formally this Laplace transform, we obtain

$$P_{\text{qu}}(Q, t) \sim \int_\Gamma \frac{du}{2\pi i} \exp \left[-uQ + \rho v_0 \gamma t^2 W \left(\frac{u}{\gamma t} \right) \right] . \quad (100)$$

Rescaling $u/(\gamma t) = x$ we get, up to pre-exponential factors,

$$P_{\text{qu}}(Q, t) \sim \int_\Gamma \frac{dx}{2\pi i} \exp \left[-\rho v_0 \gamma t^2 (-W(x) + xq) \right] , \quad \text{where } q = \frac{Q}{\rho v_0 t} . \quad (101)$$

where Γ is the Bromwich contour in the complex x -plane. Performing this integral by using a saddle-point for large t , we get

$$P_{\text{qu}}(Q, t) \sim \exp \left[-\rho v_0 \gamma t^2 \Psi_{\text{RTP}} \left(q = \frac{Q}{\rho v_0 t} \right) \right] , \quad (102)$$

with the rate function given by

$$\Psi_{\text{RTP}}(q) = \max_x [q x - W(x)] , \quad (103)$$

where $W(x)$ is given explicitly in Eq. (97). It is easy to verify that the maximum of the function $q x - W(x)$ occurs at $x = x^* = 1 - \sqrt{1 - q^2} < 1$. Since $x^* < 1$ we use the branch of $W(x)$ in the first line of Eq. (97). Substituting this value of x^* in Eq. (103) we get the result in Eq. (27). The asymptotic behaviours of this function $\Psi_{\text{RTP}}(q)$ are given in Eq. (28) and a plot of this function is shown in Fig. 5 (c). Note that for small q , i.e. $Q \ll \rho v_0 t$, $\Psi_{\text{RTP}}(q)$ behaves as $\Psi_{\text{RTP}}(q) \sim q^3/6$. Substituting this behavior in Eq. (102) gives

$$P_{\text{qu}}(Q, t) \Big|_{\text{RTP}} \sim \exp \left(-\frac{\gamma Q^3}{6 \rho^2 v_0^2 t} \right) \sim \exp \left(-\frac{Q^3}{12 \rho^2 D_{\text{eff}} t} \right) , \quad \text{where } D_{\text{eff}} = \frac{v_0^2}{2\gamma} . \quad (104)$$

On the other hand, for the diffusive case, from Eq. (20), using $\Psi_{\text{diff}}(q) \approx q^3/12$ for large q , i.e. $Q \gg \rho \sqrt{D t}$, one gets

$$P_{\text{qu}}(Q, t) \Big|_{\text{diff}} \sim \exp \left(-\frac{Q^3}{12 \rho^2 D t} \right) \quad (105)$$

Comparing these two tails (104) and (105), one sees that for the RTP, on a scale where $\rho \sqrt{D_{\text{eff}} t} \ll Q \ll \rho v_0 t$ these two behaviors match perfectly, supporting the expectation that, at large t , even for moderately large fluctuations to the right of the mean, the flux distribution for the RTP and the diffusive case coincide, once one identifies the effective diffusion constant as $D_{\text{eff}} = v_0^2/(2\gamma)$.

VI. NUMERICAL RESULTS

This section is dedicated to Monte Carlo simulations. We check numerically the analytical results previously obtained and characterize the properties of the physical realizations corresponding to large Q values.

1. The Importance Sampling strategy

In order to obtain the tails of $P_{an}(Q, t)$ and $P_{qu}(Q, t)$ we have employed Importance Sampling, a general method used to reduce the variance of observables whose expectation value is dominated by rare realizations, in this case rare trajectories. In the context of the evaluation of large deviation functions, very popular implementations of importance sampling ideas are cloning algorithms or transition path sampling [38]. Here we use an implementation of Importance Sampling, similar to transition path sampling, the details of the technique can be found in [39, 40]. Basically we sample realizations with an exponential bias on their flux, $e^{-\theta Q}$. The adjustable parameter θ allows to explore atypical realizations: a negative θ favours realizations with large Q , while a positive θ favours small Q . The sampling is done using a standard Metropolis algorithm as discussed in [39, 40] and error bars are smaller than the symbol size.

To proceed we note that the flux depends only on the particle positions at time t :

$$x_i(t) = x_i(0) + \Delta x_i(t), \quad \forall i. \quad (106)$$

We wrote this quantity as the sum of two contributions: (i) the initial (negative) position, $x_i(0) < 0$ and (ii) the total displacement, $\Delta x_i(t)$. The latter depends on the stochastic process we are considering: for the diffusive particles it is a Gaussian number of zero mean and standard deviation $\sqrt{2Dt}$. For active particles, it can be expressed as

$$\Delta x_i(t) = \pm v_0(T_1 - T_2), \quad (107)$$

where T_1 , is the total time spent moving in the initial particle direction, $T_2 = t - T_1$ the time spent in the opposite direction. The signs $+$ or $-$ correspond to the initial direction and they are chosen with equal probability. The times T_1 and T_2 are determined as follows: the run times $\tau_1, \tau_2, \dots, \tau_n$ are drawn from an exponential distribution of rate γ , the last run being the first time interval for which $\sum_{i=1}^n \tau_i > t$. Then τ_n is replaced by $t - \sum_{i=1}^{n-1} \tau_i$ and T_1, T_2 are computed.

The choice of the initial conditions is the delicate point that makes the annealed case different from the quenched one: in the annealed case, averages are performed over all initial conditions while in the quenched case the initial condition is fixed and typical. We first study the annealed case for active particles. At large times, their behavior is statistically equivalent to the one of diffusive particles with the effective constant $D_{\text{eff}} = v_0^2/(2\gamma)$. Then we discuss the quenched case and recover the exact results of previous sections. At variance with the annealed case one expects that when $Q \simeq \rho v_0 t$ active particles should have a clear non-diffusive nature even at long times. Unfortunately, the biased Monte Carlo used in this paper does not allow to sample configurations with $Q \simeq \rho v_0 t$.

A. Annealed case

The flux of RTPs depends on the evolution of the particles with an initial position $x(0)$ in $[-v_0 t, 0]$. But what is their number? Typically we expect $N \sim \rho v_0 t$, but, in the annealed case, rare realizations with large or small N can occur. To capture them we consider a large interval $[-L, 0]$ with $L \gg \rho v_0 t$ and draw $L\rho$ initial positions evenly distributed in the interval. Then only the particles with $x(0) > -v_0 t$ are evolved.

Here we study RTP with $\rho = 1, v_0 = 1, \gamma = 0.05$. At time $t = 400$, the average flux predicted by Eq. 10 is $\mu = 35.4573$, very close to the one predicted in diffusive limit $\sim \sqrt{t/(2\gamma\pi)} = 35.6825$. Then typical realizations ($\theta = 0$) are expected to be similar to the diffusive ones with $D_{\text{eff}} = v_0^2/(2\gamma) = 10$. When the bias is applied ($\theta = 1$) the sampled realizations have a larger flux, $Q \approx 93$ and it is instructive to characterize their statistical properties for RTP and diffusion.

In Fig. 6(a) we show the initial profile of particles. While for $\theta = 0$ it is flat as expected, for $\theta = -1$ it displays an accumulation of particles around the origin and total number of particles in the interval $[-v_0 t, 0]$ is much larger than $\rho v_0 t$. In Fig. 6(b) we show the histogram (normalized to the number of realizations) of displacement for particles with a positive final position. The peak for $\theta = 0$ has the same location of the peak for $\theta = -1$. The only difference is that more particles have a positive $x(t)$ for $\theta = -1$ than for $\theta = 0$. This suggests that, in the annealed case, larger values of the flux are essentially due to rare fluctuations of the initial conditions that are completely insensitive to the nature of the particle motion.

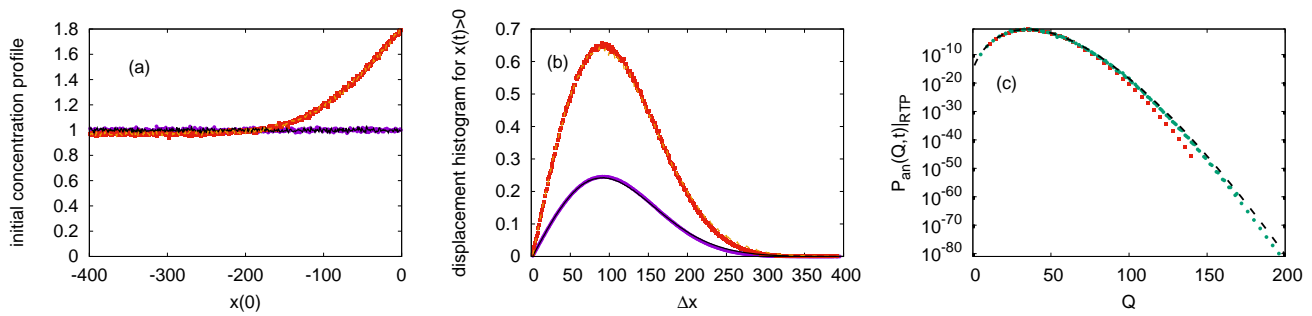


FIG. 6: Monte Carlo results for the annealed case. RTP versus Diffusion. The initial particle position is sampled with $\rho = 1$ and $L = 2000$. Particles evolve up to time $t = 400$ with $v_0 = 1, \gamma = 0.05$ for RTP (points), $D_{\text{eff}} = 10$ for diffusion (lines). We performed 10^7 realizations. (a) Initial particle concentration. For typical value of Q (violet circles/black solid lines) the profile is flat, as expected. It has been obtained by setting $\theta = 0$ as importance sampling parameter which corresponds to $Q \simeq \langle Q \rangle \approx 35.45$. For large values of Q (red squares/yellow dashed lines) we observe an accumulation of particle close to origin. There we set $\theta = -1$ as importance sampling parameter which corresponds to $Q \approx 93 \gg \langle Q \rangle$. (b) Histogram (normalized to the number of realizations) of the displacement for particles with a positive final position with $\theta = 0$, and $\theta = -1$. (c) $P_{an}(Q, t)$ vs Q ; points represent Monte Carlo results (with $L = 500$ (red squares) and $L = 2000$ (green circles)) while the dashed line is the Poisson distribution with mean $\mu = 35.4573$ (Eq. 10). In the tails the agreement improves with increasing L .

For this reason the non-gaussian tails of the flux are Poissonian both for diffusive and active particles. In Fig. 6(c) [41] we observe that the agreement between simulations and Poissonian tails increases when L is large, this confirms that the origin of anomalous fluctuations of the flux is in the rare realizations with large initial concentrations of particles close to the origin. This mechanism cannot work for the quenched case where the initial concentration is always flat.

B. Quenched case

In the quenched case the initial condition is fixed and the number of particles with an initial position in $[-v_0 t, 0]$ is always $N = \rho v_0 t$. In practice, we fix the position of the first particle x_1 using a uniform random number between 0 and $-1/(2\rho)$ and the positions of all the other $N - 1$ particles are then slaved to x_1 according to

$$x_i(0) = x_1(0) - i, \quad (108)$$

We first check the agreement between our Monte Carlo simulations and the analytical predictions. In Fig. 7 we compare the exact large deviation function $\Psi_{\text{diff}}(\frac{Q}{\rho\sqrt{Dt}})$ and the exact probability distribution function $P_{qu}(Q, t)|_{\text{diff}}$ with the ones obtained from our Monte Carlo simulations. For the quenched active case, the results are shown in Fig 8 where we also plot the large deviation function $\Psi_{\text{RTP}}(\frac{Q}{\rho v_0 t})$, using for the Monte Carlo data the definition $\Psi_{\text{RTP}}(q) = -\frac{\log P_{qu}(Q, t)}{\rho v_0 \gamma t^2}$ with $q = \frac{Q}{\rho v_0 t}$. We note that the Monte Carlo results perfectly match the predictions for both RTP and diffusion.

The difference between RTP and diffusive behaviour in the quenched case is shown in Fig. 9 (a). There we compare the exact distribution of RTP with $\rho = v_0 = 1, \gamma = 0.5$ and $t = 80$ (red) with the diffusive one with $D_{\text{eff}} = v_0^2/(2\gamma) = 1$. Both distributions deviate from the Gaussian (solid green) but they become separable from each other only at extremely small probabilities, when $Q \simeq 60 \approx \rho v_0 t$. The Importance Sampling strategy enables us to explore the non-Gaussian tails of the distribution but not the extremely rare configurations where the fingerprints of the activity are present. Indeed in Fig. 9 (b) we can hardly see a difference in histogram of the displacement of particles with positive final position between diffusion and RTP, both for $\theta = 0$ and $\theta = -3$. This is because the displacements involved are still very small compare to $v_0 t = 80$.

VII. CONCLUSION

In this paper, we have presented a general framework to study current fluctuations for non-interacting particles executing a common random dynamics in one dimension and starting from a step initial condition. The probability distribution $P(Q, t, \{x_i\})$ depends on the initial positions of the particles $\{x_i\} < 0$. The initial positions are distributed uniformly on the negative axis with a uniform density ρ . There are two different ways to perform the average over the

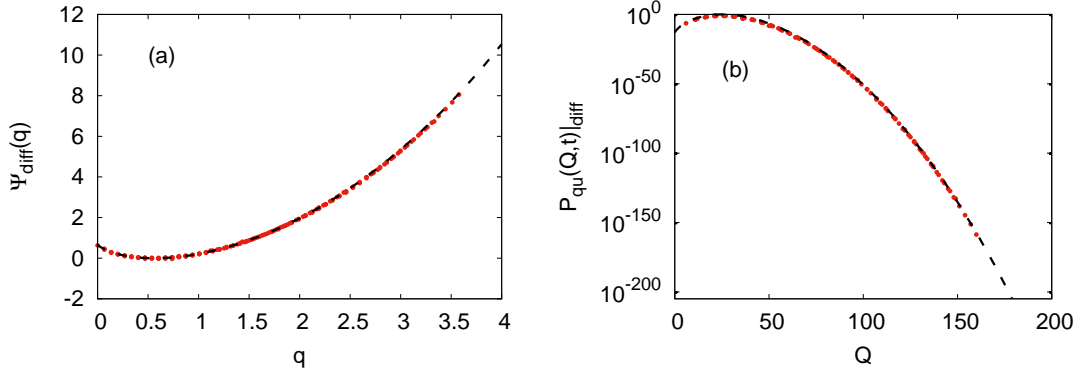


FIG. 7: Quenched case for passive dynamics. Monte Carlo simulations (red points) and exact results obtained from Mathematica (dashed black line) using Eqs. 59 and 65. Simulations were performed using $\rho = 1, D = 0.2, t = 10^4, N = 2000$. (a) $\Psi_{\text{diff}}(q)$ vs q . (b) $P_{\text{qu}}(Q, t)|_{\text{diff}}$ vs Q . The two functions are related via $P_{\text{qu}}(Q, t)|_{\text{diff}} = \exp[-\rho\sqrt{Dt}\Psi_{\text{diff}}(\frac{Q}{\rho\sqrt{Dt}})]$.

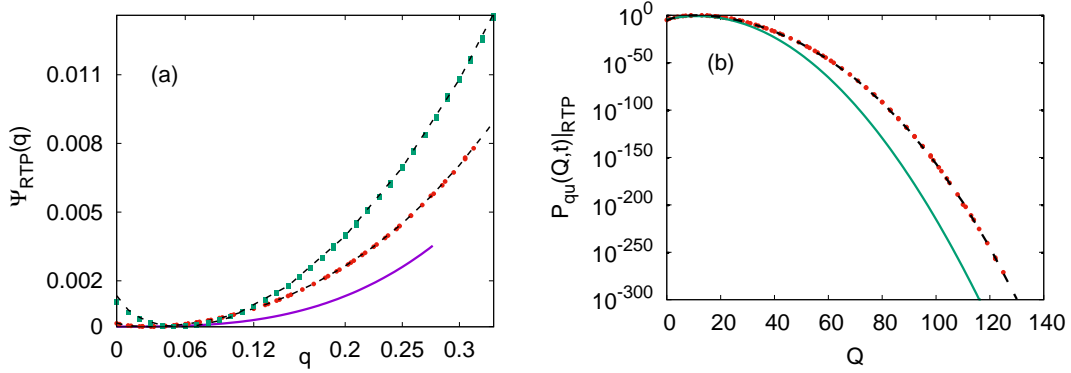


FIG. 8: Quenched case for active dynamics. Monte Carlo simulations (points) and exact results obtained from Mathematica (dashed black line) using Eqs. 81 and 89. Simulations were performed using $\rho = v_0 = 1, \gamma = 0.5$ and $t = 100$ (green squares) and $t = 400$ (red circles). (a) $\Psi_{\text{RTP}}(q)$ vs q . The violet solid curve represents $\frac{q^3}{6}$, indicating that $t = 400$ is also not large enough to see the q^3 behavior; also see Fig. 5(c) which shows that Eq. 27 becomes a good fit to the exact results only at very large times. (b) $P_{\text{qu}}(Q, t)|_{\text{RTP}}$ vs Q for $t = 400$ in the semi-log scale. Note that $P_{\text{qu}}(Q, t)|_{\text{RTP}}$ decays slower than the Gaussian expected for the typical fluctuations (green solid line). The two functions are related via $P_{\text{qu}}(Q, t)|_{\text{RTP}} = \exp[-\rho v_0 \gamma t^2 \Psi_{\text{RTP}}(\frac{Q}{\rho v_0 t})]$.

initial positions, namely (i) annealed and (ii) quenched averages, in analogy with disordered systems: here the initial condition plays the role of the disorder. In the annealed case, the distribution $P(Q, t, \{x_i\})$ is averaged directly over the initial positions. In contrast, in the quenched case, one considers the configurations of x_i 's that lead to the most likely current distribution (i.e., the *typical* current distribution). In both cases, we have shown that, for noninteracting particles, the distribution can be fully characterized in terms of the single particle Green's function, which in general will depend on the dynamics of the particles. In this article, we have focused mostly on two different dynamics: a) when the single particle undergoes simple diffusion and b) when the single particle undergoes run-and-tumble dynamics (RTP).

For the annealed case, we have shown that $P_{\text{an}}(Q, t)$, at all times, is given by a Poisson distribution, with parameter $\mu(t)$ given by the exact formula in Eq. (8). We provide exact formula for $\mu(t)$ in the RTP case (for the diffusive case this was known already from Ref. [6]). For the quenched diffusive case we show that our formalism correctly recovers the large deviation result obtained in Ref. [6] using a different approach. For the RTP case, we showed that there is a new large deviation regime with $Q \sim t$, where $P_{\text{qu}}(Q, t) \sim \exp[-\rho v_0 \gamma t^2 \Psi_{\text{RTP}}(\frac{Q}{\rho v_0 t})]$. One of the main results

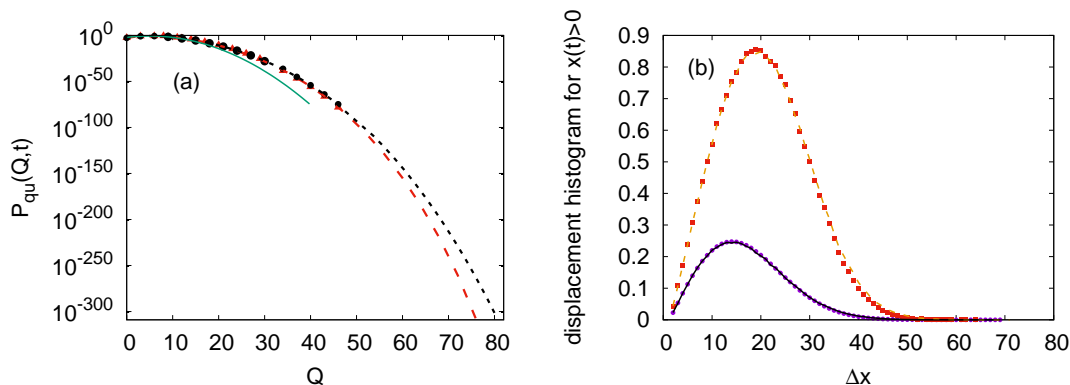


FIG. 9: (a) $P_{\text{qu}}(Q, t)$ vs Q . RTPs with $\rho = v_0 = 1, \gamma = 0.5$ and $t = 80$ (long-dashed red lines, triangles) are compared with the diffusive ones with $D_{\text{eff}} = v_0^2/(2\gamma) = 1$ (short-dashed black lines, circles). Exact results (lines) and Monte Carlo simulations (points). The solid green line represents the Gaussian valid at small Q . (b) Histogram (normalized to the number of realizations) of the displacement for particles with a positive final position with $\theta = 0$ (violet circles for RTP/ black-solid lines for diffusion), and $\theta = -3$ (red squares for RTP/ yellow-dashed lines for diffusion).

of this paper is an explicit computation of the rate function $\Psi_{\text{RTP}}(q)$ given by

$$\Psi_{\text{RTP}}(q) = q - \frac{q}{2}\sqrt{1-q^2} - \sin^{-1} \left[\sqrt{\frac{1-\sqrt{1-q^2}}{2}} \right], \quad 0 \leq q \leq 1. \quad (109)$$

Our method gives access to another physical observable, namely the probability of an extremely rare event that there is no particle on the right side of the origin at time t . We have shown that this is just the probability of having zero flux up to time t , i.e. $P(Q = 0, t)$, both for the annealed and the quenched case. For the annealed case, this is just $P_{\text{an}}(Q = 0, t) = e^{-\mu(t)}$. For the quenched case, we have that, both for the diffusive and RTP cases, this probability decays at late times as a stretched exponential $P_{\text{qu}}(Q = 0, t) \sim e^{-\bar{\alpha}\sqrt{D_{\text{eff}}}t}$, where we computed the constant $\bar{\alpha} = 0.675336\dots$ analytically [see Eq. (22)]. For diffusive particles, $D_{\text{eff}} = D$ while for RTP's, $D_{\text{eff}} = v_0^2/(2\gamma)$.

We have also verified our analytical predictions by numerical simulations. Computing numerically the large deviation function is far from trivial. Even for the diffusive case the large deviation function predicted for $P(Q, t)$ (both annealed and quenched) in Ref. [6] was never verified numerically. In this paper, we used a sophisticated importance sampling method to compute numerically this large deviation function in the diffusive case up to an impressive accuracy of order 10^{-200} . We further used the same technique to compute the large deviation function in the RTP case.

The formalism developed in this paper can be easily generalized in different directions. For instance, one can compute the flux distribution exactly for the case where there are, initially, arbitrary densities ρ_{left} and ρ_{right} to the left and to the right of the origin respectively, both the diffusive and for the RTP cases. One could also generalise this result in higher dimensions, with step-like initial conditions, where for instance one region of the space is initially occupied by particles with uniform density. For the diffusive case, the flux distribution in the presence of hard-core repulsions between particles was studied in Ref. [7] (for the simple symmetric exclusion process). It would be interesting to see whether our formalism can be generalized to study the flux distribution for RTP's with hard core repulsions.

Acknowledgments

We acknowledge support from the project 5604-2 of the Indo-French Centre for the Promotion of Advanced Research (IFCPAR).

-
- [1] T. Bodineau and B. Derrida, *Current fluctuations in non-equilibrium diffusive systems: an additivity principle*, Phys. Rev. Lett. **92**, 180601 (2004).
 [2] L. Bertini, A. De Sole, D. Gabrielli, G. Jona-Lasinio, and C. Landim *Current fluctuations in stochastic lattice gases*, Phys. Rev. Lett. **94**, 030601 (2005).

- [3] L. Bertini, A. De Sole, D. Gabrielli, G. Jona-Lasinio, C. Landim, *Non equilibrium current fluctuations in stochastic lattice gases*, J. Stat. Phys. 123237-276 (2006).
- [4] S. Prolhac and K. Mallick, *Current Fluctuations in the exclusion process and Bethe Ansatz*, J. Phys. A: Math. Theor. **41** 175002 (2008).
- [5] C. Appert-Rolland, B. Derrida, V. Lecomte, F. Van Wijland, *Universal cumulants of the current in diffusive systems on a ring*, Phys. Rev. E. **78**, 021122 (2008).
- [6] B. Derrida and A. Gerschenfeld, *Current Fluctuations in One Dimensional Diffusive Systems with a Step Initial Density Profile*, J. Stat. Phys. **137**, 978 (2009).
- [7] B. Derrida and A. Gerschenfeld, *Current Fluctuations of the One Dimensional Symmetric Simple Exclusion Process with Step Initial Condition*, J Stat Phys **136**, 1 (2009).
- [8] M. Prähofer and H. Spohn, *Current fluctuations for the totally asymmetric simple exclusion process*, In and out of equilibrium, ed. V. Sidoravicius, Progress in Probability **51**, 185-204, Birkhauser Boston (2002).
- [9] P. L. Krapivsky, B. Meerson, *Fluctuations of current in nonstationary diffusive lattice gases*, Phys. Rev. E **86**, 031106 (2012).
- [10] H. C. Berg, *E. coli in Motion* (Springer, 2014).
- [11] J. Tailleur and M. E. Cates, *Statistical mechanics of interacting Run-and-Tumble bacteria*, Phys. Rev. Lett. **100**, 218103 (2008).
- [12] K. Martens, L. Angelani, R. Di Leonardo, and L. Bocquet, *Probability distributions for the run-and-tumble bacterial dynamics: An analogy to the Lorentz model*, Eur. Phys. J. E **35**, 84 (2012).
- [13] A. E. Patteson, A. Gopinath, M. Goulian, P. E. Arratia, *Running and tumbling with E. coli in polymeric solutions*, Sci Rep. 2015 Oct 28; 5:15761. doi: 10.1038/srep15761.
- [14] W. Stadje, *The exact probability distribution of a two-dimensional random walk*, J. Stat. Phys. **46**, 207 (1987).
- [15] G. H. Weiss, *Some applications of persistent random walks and the telegrapher's equation*, Physica A: Statistical Mechanics and its Applications **311**, 381 (2002).
- [16] E. Fodor, C. Marchetti, Lecture notes for the international summer school "Fundamental Problems in Statistical Physics" held in Bruneck, Physica A **504**, 106 (2018).
- [17] C. Bechinger, R. Di Leonardo, H. Löwen, C. Reichhardt, G. Volpe and G. Volpe, *Active particles in complex and crowded environments*, Rev. Mod. Phys. **88**, 045006 (2016).
- [18] M. E. Cates, J. Tailleur, *Motility-Induced Phase Separation*, Annu. Rev. Condens. M. P. **6**, 219 (2015).
- [19] A. P. Solon, Y. Fily, A. Baskaran, M. E. Cates, Y. Kafri, M. Kardar, J. Tailleur, *Pressure is not a state function for generic active fluids* Nature Phys. **11**, 673 (2015).
- [20] A. B. Slowman, M. R. Evans and R. A. Blythe, *Jamming and attraction of interacting run-and-tumble random walkers*, Phys. Rev. Lett. **116**, 218101 (2016).
- [21] G. Gradenigo, S. N. Majumdar, *A first-order dynamical transition in the displacement distribution of a driven run-and-tumble particle*, J. Stat. Mech.: Theor. Exp. 053206, (2019).
- [22] P. Hänggi, P. Jung, *Colored noise in dynamical systems*, Adv. Chem. Phys. **89**, 239 (1995).
- [23] A. Dhar, A. Kundu, S. N. Majumdar, S. Sabhapandit, G. Schehr, *Run-and-tumble particle in one-dimensional confining potentials: Steady-state, relaxation, and first-passage properties*, Phys. Rev. E **99**, 032132 (2019).
- [24] E. Mallmin, R. A. Blythe and M. R. Evans, *Exact spectral solution of two interacting run-and-tumble particles on a ring*, J. Stat. Mech.: Theor. Exp. 013204, (2019).
- [25] F. J. Sevilla, A. V. Arzola and E. P. Cital, *Stationary superstatistics distributions of trapped run-and-tumble particles*, Phys. Rev. E **99**, 012145 (2019).
- [26] Y. Ben Dor, E. Woillez, Y. Kafri, M. Kardar, A. P. Solon, *Ramifications of disorder on active particles in one dimension*, preprint arXiv:1908.00568 (2019).
- [27] J. Masoliver, K. Lindenberg, and B. J. West, *First-passage times for non-Markovian processes: Correlated impacts on a free process*, Phys. Rev. A **34**, 1481 (1986).
- [28] L. Angelani, R. Di Leonardo and M. Paoluzzi, *First-passage time of run-and-tumble particles*, Euro. J. Phys. E **37**, 59 (2014).
- [29] L. Angelani, *Run-and-tumble particles, telegrapher's equation and absorption problems with partially reflecting boundaries*, J. Phys. A: Math. Theor. **48**, 495003 (2015).
- [30] K. Malakar *et al*, *Steady state, relaxation and first-passage properties of a run-and-tumble particle in one-dimension* J. Stat. Mech. (2018) 043215
- [31] T. Demaerel and C. Maes, *Active processes in one dimension*, Phys. Rev. E. **97**, 032604 (2018).
- [32] P. Le Doussal, S. N. Majumdar, G. Schehr, *Non-crossing run-and-tumble particles on a line*, arXiv:1902.06176 (2019).
- [33] P. Singh, A. Kundu, *Generalised "Arcsine" laws for run-and-tumble particle in one dimension*, J. Stat. Mech., 083205 (2019).
- [34] M. R. Evans and S. N. Majumdar, *Run and tumble particle under resetting: a renewal approach*, J. Phys. A: Math. Theor. **51**, 475003 (2018).
- [35] For a recent review on stochastic resetting, see M. R. Evans, S. N. Majumdar, G. Schehr, *Stochastic resetting and applications*, J. Phys. A: Math. Theor. in press <https://doi.org/10.1088/1751-8121/ab7cfe> (2020).
- [36] B. Lacroix-A-Chez-Toine, J. Andres Monroy Garzon, C. Sebastian Hidalgo Calva, I. Perez Castillo, A. Kundu, S. N. Majumdar, G. Schehr, *Intermediate deviation regime for the full eigenvalue statistics in the complex Ginibre ensemble*, Phys. Rev. E **100**, 012137 (2019).
- [37] B. Lacroix-A-Chez-Toine, S. N. Majumdar, G. Schehr, *Rotating trapped fermions in two dimensions and the complex*

- Ginibre ensemble: Exact results for the entanglement entropy and number variance*, Phys. Rev. A **99**, 021602(R) (2019).
- [38] C. Giardinà, J. Kurchan, V. Lecomte, J. Tailleur, *Simulating rare events in dynamical processes*, J. Stat. Phys., **145**, 787, (2011).
- [39] A. K. Hartmann *et al*, *High-precision simulation of the height distribution for the KPZ equation*, Euro. Phys. Lett. **121** (2018).
- [40] A. K. Hartmann, *Large-deviation properties of largest component for random graphs*, Eur. Phys. J. B **84**, 627 (2011).
- [41] Note that to obtain a reliable histogram one has to re-weight the sampled values of Q by a factor $Z(\theta)e^{\theta Q}$. $Z(\theta)$ is a normalization constant that is determined following the method explained in [39, 40].